Mott insulator breakdown through pattern formation

Pedro Ribeiro,[1] Andrey E. Antipov,[2] and Alexey N. Rubtsov[1]

[1] *Russian Quantum Center, Novaya street 100 A, Skolkovo, Moscow area, 143025 Russia**

[2] *Department of Physics University of Michigan, Randall Laboratory, 450 Church Street, Ann Arbor, MI 48109-1040*

We study the breakdown of a Mott insulator with the thermodynamic imbalance induced by an applied bias voltage. By analyzing the instabilities of the magnetic susceptibility, we describe a rich non-equilibrium phase diagram, obtained for different applied voltages, that exhibits phases with a spatially patterned charge gap. For a finite voltage, smaller than the value of the equilibrium Mott gap, the formation of patterns coincides with the emergence of mid-gap states contributing to a finite steady-state conductance. We discuss the experimental implications of this new scenario of Mott breakdown.

PACS numbers: 72.10.-d, 71.27.+a, 72.20.-i, 71.30.+h

arXiv:1412.8644v1 [cond-mat.str-el] 30 Dec 2014

Pattern formation, also known as self-organization, refers to the occurrence of spatial-structured steady-states in non-linear systems under out of equilibrium external conditions [1]. A textbook illustration is the Rayleigh–Bénard convection, but examples are found ubiquitously in physical, chemical as well as in biological systems [2, 3].

In semiconductors, pattern formation is a hallmark of the voltage-driven non-equilibrium phase transition from insulating to the metallic state [4], where moving patterns arise near phase boundaries that contribute to the finite conductivity of the system. A seminal experiment, revealing pattern formation in strongly correlated systems [5] reported a current-induced pattern formation in a quasi-one dimensional organic charge-transfer complex, on the verge of Mott breakdown. A non-linear I-V characteristic was reported in a low-resistance state characterized by a striped charge pattern, before the switching to metallic regime. Recently, experimental results for spinor Bose-Einstein condensates [6] and, theoretical studies of polariton condensates [7, 8] also reported patterned phases.

Non-equilbrium dynamics of strongly correlated quantum many-body systems have been recently receiving an increased attention due to a rich interplay between electronic kinetics, interaction and non-equilibrium conditions. Major experimental progress was driven forward by a tight control of the dynamics in cold atomic setups [9, 10] and pump-probe experiments [11, 12]. On the theory side, progress been done in understanding thermalization and dissipation [13–15], universal aspects of non-equilibrium phase transitions [16–24] and the development of involved computational methods [25–29] and techniques [30–32]. In particular, the study of out-of-equilibrium properties of the Hubbard model has been an active research area [30, 33–35]. Interesting dynamical transitions between small and large interaction quenches where shown to occur at half-filling [31, 32, 36–38]. Transport properties at finite temperature [39] and in the presence of Markovian dissipation [40, 41] have been investigated.

A key problem is the understanding of the transition from a Mott insulator to a current-carrying state upon applied an increasing voltage bias to coupled external leads. The generated electro-chemical gradients induce two effects of rather different nature: (i) a thermodynamic-imbalance depending on the distribution functions of the leads and (ii) the coupling of the charged particles to the electric field created by the voltage drop.

The breakdown of a Mott insulator induced by effect (ii) recently received important contributions. Using Peierls substitution argument, (ii) can be studied on a system with periodic boundary conditions pierced by a linear-in-time magnetic flux, eliminating the need of explicitly treating the reservoirs and making it amenable to be tackled by Lanczos [42], DMRG [43] and DMFT [34, 44, 45] methods. These studies revealed a qualitative scenario [42] interpreted as the many-body analog of the Landau-Zener (LZ) mechanism observed in band insulators. The LZ energy scale sets a threshold $V_{\rm th} \sim \Delta^2 L/W$, with Δ being the Mott gap, L – the system's linear size and W – the bandwidth, above which a field-induced metallic phase sets in. Zener's formula yields $V_{\rm th}/L \gg \Delta$ overestimating experimental values of threshold fields.

The combined effect of (i) and (ii) have also been recently addressed [46–48]. As (i) requires the explicit treatment of the reservoirs, non-equilibrium Green's functions approaches were employed. (ii) was treated within the Hartree approximation with a fixed antiferromagnetic order, precluding any pattern formation. The results are compatible with a current-voltage characteristics of the form $J \simeq V e^{-V_{\rm th}/V}$. A thorough study [48], carried out at $T = 0$ in the presence of long-range Coulomb interactions, pointed out that the dominant effect depends on the ratio between the correlation length in the insulating phase ξ and the size of the insulating region L. For $\xi/L \gg 1$, (i) leads to $V_{\rm th} \sim \Delta$; for $\xi/L \ll 1$ (ii) dominates and the LZ scenario is recovered.

In this letter, we address out-of-equilibrium properties of Hubbard chain due to thermodynamic-imbalance (i). We describe the appearance of mobile carriers that contribute to the screening of the field. The leads pro-

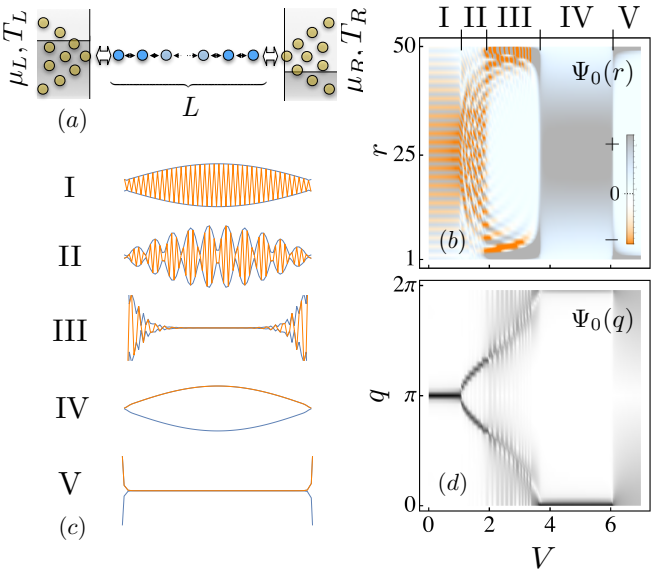

Figure 1. (a) Schematic view of the physical setup. (b) Density plot of the most unstable mode $\Psi_0(r)$plotted as a function of the bias V for $\Gamma = 0.25$, $T = 0.25$ and $L = 50$. The phase labels I,...,V point to qualitatively different behavior of $\Psi_0(r)$. (c) Typical spatial dependence of $\Psi_0(r)$ in each phase (orange line), plotted for $L = 80$. The blue line depicts the envelope function. (c) Density plot of the Fourier transform $\Psi_0(q)$ of $\Psi_0(r)$ as a function of q computed for $L = 50$.

vide, at the same time, the non-equilibrium conditions and an intrinsically non-Markovian [49] dissipative environment. We compute the instabilities of the system to spatially modulated spin patterns and identify a rich set of candidate phases, among which examples of pattern formation, analyzing their properties in the strong nonlinear regime. We put forward a scenario of the Mott breakdown through the emergence of conducting midgap states coinciding with the appearance of patterns for $V_{\rm th} \lesssim \Delta$. Our results are of relevance to pattern formation in quasi-one dimensional organic compounds [5].

We consider the interacting system S, in Fig. 1-(a), consisting of a chain coupled to metallic reservoirs. The Hamiltonian can be decomposed as $H = H_{\rm S} + H_{\partial {\rm S}} + H_{\bar{\rm S}}$, where

$$H_{\rm S} = -t \sum_{\langle \boldsymbol{r},\boldsymbol{r}'\rangle,s} c^\dagger_{\boldsymbol{r}s} c_{\boldsymbol{r}'s} + \frac{U}{2} \sum_{\boldsymbol{r}} \left(n_{\boldsymbol{r}} - 1\right)^2 \qquad (1)$$

is the Hamiltonian of the system consisting of a fermionic Hubbard chain, with s labeling spin degrees of freedom and $n_{\boldsymbol{r}} = \sum_\sigma c^\dagger_{\boldsymbol{r}s} c_{\boldsymbol{r}s}$. The hopping matrix element between nearest neighbor sites, $t = 1$, is taken to be the energy unit. $H_{\bar{\rm S}} = \sum_{\alpha,s,l} d^\dagger_{l\alpha s} \epsilon_{l,\alpha} d_{l\alpha s}$ is the Hamiltonian of the reservoirs, with $l = L, R$ labeling the reservoir and α – the reservoir's single-particle modes. The density of states of the leads is taken to be the one of a wide band metallic lead, i.e. a constant ρ, within all the considered energy scales for both leads. The system-reservoirs coupling is described by the hopping term $H_{\partial {\rm S}} = \sum_{\alpha,s,l} v\, d^\dagger_{l\alpha s} c_{\boldsymbol{r}_l,s} + {\rm h.c.}$, where $\boldsymbol{r}_{L,R}$ are the sites at the extremities of the chain and v is the hopping amplitude taken to be spin independent. We consider reservoirs at temperature T that are characterized by the same hybridization $\Gamma = \pi v^2 \rho$ for simplicity.

We employ a non-equilibrium mean-field approach, that while providing only a qualitative description of the 1d model, allows to probe instabilities of the system towards the formation of gapped phases. The procedure to obtain the mean-field equations and the magnetic susceptibility is standard and is given in the SI for completeness. Here we outline the main steps. Working on the Keldysh contour we use the identity $\frac{U}{2}\sum_{\boldsymbol{r}} \left(n_{\boldsymbol{r}} - 1\right)^2 = -\frac{3}{4} U \left(\boldsymbol{S}_{\boldsymbol{r}}.\boldsymbol{S}_{\boldsymbol{r}} - 1\right)$, with $\boldsymbol{S}_{\boldsymbol{r}} = \frac{1}{2} c^\dagger_{\boldsymbol{r},s} \boldsymbol{\sigma}_{ss'} c_{\boldsymbol{r},s'}$, and insert a 3-component time dependent order-parameter $\boldsymbol{\phi}(t)$ to decouple the interaction term in the spin-density wave channel $\frac{3}{4} U \boldsymbol{S}_{\boldsymbol{r}}.\boldsymbol{S}_{\boldsymbol{r}} \rightarrow \boldsymbol{S}_{\boldsymbol{r}}.\boldsymbol{\phi}_{\boldsymbol{r}} + \frac{1}{3U} \boldsymbol{\phi}_{\boldsymbol{r}}.\boldsymbol{\phi}_{\boldsymbol{r}}$. Assuming a wide-band limit, we then integrate out the non-interacting reservoirs introducing a local self-energy contribution for the interacting c electrons with non-zero components (see SI-sec.): $\Sigma^{R/A}_{\boldsymbol{r}=\boldsymbol{r}_l,\boldsymbol{r}'=\boldsymbol{r}_l}(t,t') \simeq \mp i\Gamma\delta(t-t')$, $\Sigma^{K}_{\boldsymbol{r}=\boldsymbol{r}_l,\boldsymbol{r}'=\boldsymbol{r}_l}(t,t') \simeq -2i\Gamma \int \frac{d\varepsilon}{2\pi} \tanh\left[\frac{\beta_l}{2}(\varepsilon - \mu_l)\right] e^{-i\varepsilon(t-t')}$. Integrating out the c electrons, we arrive to the action for the order-parameter $\boldsymbol{\phi}(t)$ alone. We use the Keldysh rotation of the time-dependent order parameter to the quantum and classical components ($\boldsymbol{\phi}_{c,\boldsymbol{r}}$,$\boldsymbol{\phi}_{q,\boldsymbol{r}}$) and by varying the action with respect to these fields we obtain their mean field values:

$$\begin{aligned} \boldsymbol{\phi}_{c,\boldsymbol{r}}(t) &= -i\frac{3U}{4}\frac{1}{\sqrt{2}} {\rm tr}\left[G^K_{\boldsymbol{rr}}(t,t)\,\boldsymbol{\sigma}\right] \\ \boldsymbol{\phi}_{q,\boldsymbol{r}}(t) &= 0, \end{aligned} \qquad (2)$$

where $G^K_{\boldsymbol{rr}}(t,t)$ is the Keldysh component of the local c-electron Green's function. We focus on the steady state regime $\boldsymbol{\phi}_{c,\boldsymbol{r}}(t) = \boldsymbol{\phi}_{c,\boldsymbol{r}}$. At the mean-field level, the excitation spectrum is given by the non-hermitian mean-field operator

$$K = -t \sum_{\langle \boldsymbol{r},\boldsymbol{r}'\rangle,s} c^\dagger_{\boldsymbol{r}s} c_{\boldsymbol{r}'s} - i\Gamma \sum_{l,s} c^\dagger_{\boldsymbol{r}_l s} c_{\boldsymbol{r}_l s} - \\ - \frac{1}{\sqrt{2}} \sum_{\boldsymbol{r}ss'} \left(\boldsymbol{\sigma}_{ss'}.\boldsymbol{\phi}_{c,\boldsymbol{r}}(t)\right) c^\dagger_{\boldsymbol{r}s} c_{\boldsymbol{r}s'}. \qquad (3)$$

The retarded Green's function is obtained as a function of the left- ($\langle\tilde{\alpha}|$) and right- ($|\alpha\rangle$) eigenvectors of K with complex eigenvalues λ_α (${\rm Im}\lambda_\alpha < 0$): $G^R(\omega) = \sum_\alpha |\alpha\rangle (\omega - \lambda_\alpha)^{-1} \langle\tilde{\alpha}|$. The Keldysh component, derived in detailed in the SI, is obtained in a similar way.

Fluctuations around the mean-field further provide a stability analysis for the saddle-point solutions. In order to investigate the possible steady-states that can

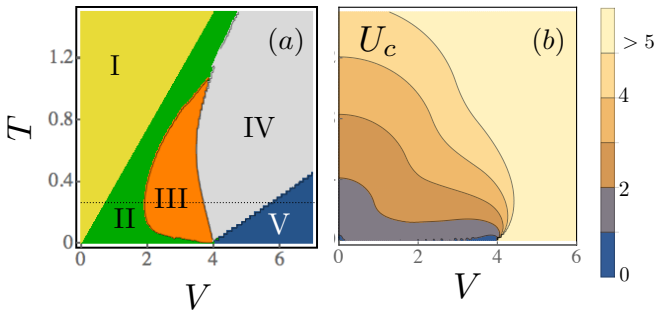

Figure 2. (a) Phase diagram as a function of V and T computed for $\Gamma = 0.25$ and $U = U_c(T,V)$. The dashed line corresponds to the plots (b) and (c) of Fig.1. (b) Values of U_c for which the first instability arises as a function of V and T, for $\Gamma = 0.25$ and $L = 50$.

be realized under non-equilibrium conditions we compute the spin susceptibility χ in the disordered state ($\boldsymbol{\phi}_{c,\boldsymbol{r}} = 0$) and analyze the first unstable modes arising upon increasing U. The retarded spin susceptibility $\chi^R_{ii';\boldsymbol{r}\boldsymbol{r}'}(t,t') = -i\Theta(t-t')\left\langle\left\{S^i_{\boldsymbol{r}}(t), S^{i'}_{\boldsymbol{r}'}(t')\right\}\right\rangle$ (with $i,i' = x,y,z$) is given by the RPA-type expression and in the steady state reads

$$\left[\chi^R_{ii'}(\omega)\right]^{-1}_{\boldsymbol{r}\boldsymbol{r}'} = \delta_{ii'}\left[-\frac{2}{3U}\delta_{\boldsymbol{r}\boldsymbol{r}'} - \Xi^R_{\boldsymbol{r}\boldsymbol{r}'}(\omega)\right], \qquad (4)$$

where $\Xi^R_{rr'}(t,t') = -i\frac{1}{2}\mathrm{tr}[G^A_{\boldsymbol{r}'\boldsymbol{r}}(t',t)\,G^K_{\boldsymbol{r}\boldsymbol{r}'}(t,t') + G^K_{\boldsymbol{r}'\boldsymbol{r}}(t',t)\,G^R_{\boldsymbol{r}\boldsymbol{r}'}(t,t')]$ is the bare bubble diagram computed at $\boldsymbol{\phi}_{c,\boldsymbol{r}} = 0$ and $G^{R/A}_{\boldsymbol{r}\boldsymbol{r}'}(t,t')$ are the spatially resolved retarded/advanced components of the Green's function of the c-electrons.

Upon increasing U, the eigenvalues of $\chi^R(\omega)$ as a functions of ω, may develop poles in the upper-half of the complex plane. When this occurs, small perturbations in the direction of the corresponding eigenmode of $\chi^R(\omega)$ grow exponentially in time until anharmonic mode-coupling terms start to be relevant. This process signals an instability of the system. The new stable phase, arising for $U > U_c$, is expected to develop the spatial structure of the lowest eigen-mode of $\chi^R(\omega)$, at least for U sufficiently close to U_c. In the following we assume that unstable modes first occur for steady-state solutions i.e. at $\omega = 0$. The unstable mode corresponds to the most negative eigenvalue λ^{Ξ}_0 of $\boldsymbol{\Xi}^R(\omega = 0)$ and its spatial configuration is given by the corresponding eigenvector $\Psi_0(r)$.

At equilibrium, and for periodic boundary conditions, $\Psi_0(r) = \frac{1}{\sqrt{L}}e^{iQr}$, with $Q = \pi$, signals the instability to the antiferromagneticaly ordered phase. This picture is essentially unchanged in the presence of open boundary conditions with the order parameter amplitude typically getting distorted near the boundaries of the system.

Figs. 1-(b,c) depict the typical spatial structure of steady state $\Psi_0(r)$ obtained upon varying the bias voltage V. Five different phases (labeled by I,...,V) can be observed, corresponding to qualitatively different features of $\Psi_0(r)$. Fig. 1-(d) depicts a contour plot of the Fourier transform $\Psi_0(q)$ of $\Psi_0(r)$ showing that the different phases correspond to different wave vectors Q for which $|\Psi_0(Q)|$ is maximal. Phase I occurs for low voltages $V < V_{\mathrm{AF}}$ and $T > 0$ and occupies a region where the antiferromagnetic phase corresponds to the first instability. The order parameter is maximal in the center of the system. The emergence of patterns is visible in phase II ($V_{\mathrm{AF}} < V < V_{\mathrm{loc}}$), where the spin-susceptibility instability corresponds to an ordered state with wave vectors $q = \pm Q$, with Q varying between π, for $V = V_{\mathrm{AF}}$, and $Q \leq 0$, for $V = V_{\mathrm{loc}}$. Phase III ($V_{\mathrm{loc}} < V < V_{\mathrm{F}}$) corresponds to a modulated phase, with $Q \neq 0, \pi$, exponentially localized near the leads. Phase IV ($V_{\mathrm{F}} < V < V_0$) is a ferromagnetic phase with an envelope function that is maximal at the center of the system. Finally, phase V corresponds to an essentially disordered phase ($\phi = 0$) with the order parameter amplitude being localized in the first few sites near the leads.

Fig. 2-(a) shows the phase diagram in the $V-T$ plane for $\Gamma = 0.25$ near $U = U_c(T,V)$ for which the first instability arises. At $T = 0$ the anti-ferromagnetism of phase I is unstable under any finite bias voltage giving place to the modulated phase II. Moreover, at zero temperature no ferromagnetic phase is present yielding a direct transition form II to the disordered phase V. The localized modulated phase III is present only for intermediate temperatures. For sufficiently high temperatures, within the range of temperatures and voltages studied, only phase I, II and IV are observed. The critical value of U, given by $U_c = -2/(3\lambda^{\Xi}_0)$ after Eq.(4), is plotted in Fig.(2)-(b). for a system with $L = 50$. For low temperature, this quantity is subjected to strong finite size corrections. Care must be taken extrapolating to the thermodynamic limit, nonetheless we verify that for $T \to 0$ and $L \to \infty$ one has $U_c \to 0$.

In order to verify the existence of well-defined patters at $U > U_c$ and describe their spatial structure, the linear response RPA-type description is insufficient, as nonlinear terms in Eq.(2) start to play an important role and have to be taken into account. In this regime, the mean-field solution for the order parameter $\boldsymbol{\phi}$ is obtained solving the self-consistent relation in Eq.(2). The procedure is done iteratively allowing only for collinear magnetized states, i.e. $\langle \boldsymbol{S}_{\boldsymbol{r}}\rangle \propto \hat{\boldsymbol{e}}_z$. Fig.3-(a) shows the spatial structure of $\phi(r)$ obtained in this way. The considered value of $U = 3.8$ corresponds to an equilibrium ($V = 0$) Mott gap of $\Delta = 2|\phi| \simeq 3.2$. Out of equilibrium, phases III-V are absent and the range of values of V for which phase II arises is reduced with respect to the diagram of Fig. 2-(a). Nevertheless, a modulated solution can be found deep into the non-linear regime. Fig.2-(b) depicts the maximum value of the order parameter amplitude ϕ_{Max} showing that phase II transits directly to the disordered

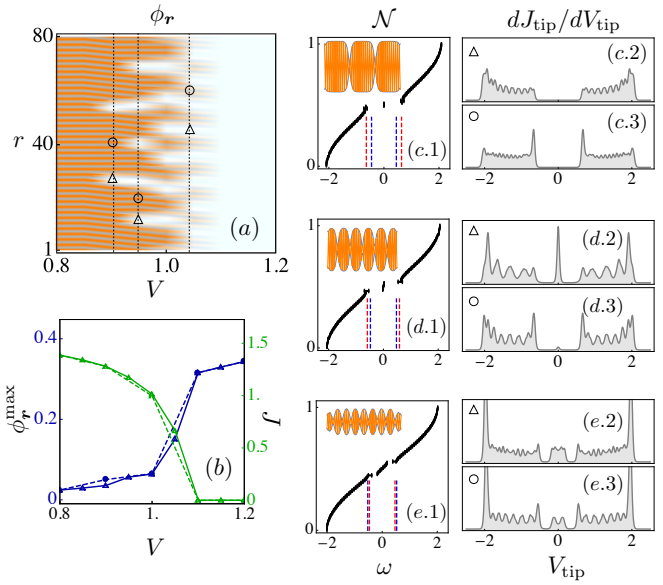

Figure 3. Properties for $U > U_c$ obtained for $\Gamma = 0.25$, $T = 0.25$, $U = 3.8$ corresponding to an equilibrium ($V = 0$) Mott gap of $\Delta = 2\,|\phi| \simeq 3.2$. (a) Density plot of $\Phi\,(r)$ plotted as a function of V for $L = 80$. The lines and markers label the specific values of Figs. (c-e). (b) Maximum value of the order parameter $\phi_{\rm Max} = \max_r |\phi\,(r)|$ (green) and particle current thought the chain J (blue) as a function of V for $L = 80$ (open triangles) and $L = 120$ (full circles). (c.1) Integrated density of states $\mathcal{N}\,(\omega) = \sum_\alpha \Theta\,(\omega - {\rm Re}\lambda_\alpha)$ for $V = 0.9$ and $L = 80$, the thickness of the black line is given by ${\rm Im}\lambda_\alpha$. The red-dashed lines correspond to $\omega = \pm\Phi_{\rm Max}$ and the blue-dashed lines to $\omega = \pm V/2$. The inset depicts the spatial dependence of $\phi\,(r)$. (c.2-3) Differential conductance $dJ_{\rm tip}/dV_{\rm tip}$ obtained by an STM tip, computed for $T_{\rm tip} = 0.02$, placed at position $\boldsymbol{r}$, for $\boldsymbol{r} = 27$ (c.2) $\boldsymbol{r} = 41$ (c.3), corresponding to a minimum and a maximum of the order parameter amplitude. (d.1-3) Same as (c.1-3) for $V = 0.95$, $\boldsymbol{r} = 12$ and $\boldsymbol{r} = 19$. (e.1-3) Same as (c.1-3) for $V = 1.05$, $\boldsymbol{r} = 45$ and $\boldsymbol{r} = 59$.

phase $\phi = 0$ upon increasing V.

Fig. 2-(b) shows also the values of the particle current through the system. A relatively low current in phase I is followed by a quick rise of current during phase II and a linear I-V characteristics in the disordered phase. Figs. 2-(c-e.1) show the integrated steady state density of states in phase II. One observes that upon increasing V a new band of conducting states arises, corresponding to single particle-energies $-V/2 < {\rm Re}\lambda_\alpha < V/2$. The appearance of such states is responsible for the current increase in phase II. This phase ceases to exist when V becomes of the order of the of the inter-band gap, roughly given by $\phi_{\rm Max}$, corresponding a complete filling of the gap by conducting states. The I-V characteristics can thus be used to discriminate between different behaviors.

To further characterize these states we monitor the differential conductivity that is measured by an STM tip placed over site $\boldsymbol{r}$. Assuming a wide-band metallic tip with constant DOS $\rho_{\rm tip}$, weakly coupled to the chain at position $\boldsymbol{r}$ by an hopping amplitude $t_{\rm tip}$, one obtains the standard linear-response expression

$$\frac{dJ_{\rm tip}}{dV_{\rm tip}} \propto -\int d\omega \frac{\beta_{\rm tip}/2}{\cosh\left[\beta_{\rm tip}\left(\omega - V_{\rm tip}\right)\right] + 1} \rho_{\boldsymbol{r}}\left(\omega\right)$$

where $\rho_{\boldsymbol{r}}\left(\omega\right) = {\rm tr}\left[G^R_{\boldsymbol{r},\boldsymbol{r}}\left(\omega\right) - G^A_{\boldsymbol{r},\boldsymbol{r}}\left(\omega\right)\right]/\left(-2\pi i\right)$ is the local DOS of the chain at site $\boldsymbol{r}$, $\beta_{\rm tip}$ and $V_{\rm tip}$ are respectively the tip's inverse temperature and chemical potential. Figs. 3 (c-e.2-3) show $dJ_{\rm tip}/dV_{\rm tip}$ for sites corresponding to minima and maxima of the order parameter for 3 values of V within phase II. The band of conducting states is can clearly be seen arising within the gap. The local DOS for $|V_{\rm tip}| < \phi_{\rm Max}$ increases or decreases, depending on whether a position corresponding to a minimum or a maximum of the order parameter amplitude is monitored.

To summarize, we have described a scenario of the Mott breakdown, induced by the pattern formation in a correlated electronic system under strong non-equilibrium conditions imposed by a finite bias voltage. The development of a conducting phase occurs at voltages, smaller than the value of the charge gap, and is characterized by the emergence of the mid-gap states. The thermodynamic imbalance imposed by a finite applied voltage generates a rich set of behaviors, among which examples of non-equilibrium spatially-induced patterned phases. Such phases, well studied in classical systems, and recently predicted in systems with Markovian dissipation [7, 8], are here reported for the fermionic Hubbard model with a non-Markovian environment and are shown to exist down to zero temperature. The suggested mechanism can be tested experimentally monitoring current transport across the system and by STM measurements, spatially resolving the modulated charge gap.

Our considerations capture characteristic features of the breakdown of the organic charge insulator, reported in Ref. [5]. The transition to the conducting state, accompanied by the formation of alternating carrier rich stripes, is reproduced with a similar I-V characteristic. Important differences, such as a diffusive electronic transport and the long-range Coulomb interactions within the Mott phase, hinder a quantitative prediction of the experimental parameters.

The present results suggest that, as in the case of classical systems, patterned phases can be ubiquitous in the presence of interactions and spatially non-uniform out of equilibrium conditions. In 1d, the phase transitions obtained at the mean-field level should instead correspond to crossovers. In the same way, the calculated magnetic order is likely to correspond to a disordered phase with slow power-law decaying spin-spin correlation functions with a voltage-dependent Q. The emergent order, seen at the mean-field level, can otherwise be stabilized by weakly coupling multiple chains. For electronic systems with higher dimensionality, such as films and bulk compounds, pattern formation should naturally

take place. These effects should depend on the orientation of the non-equilibrium drive with respect to the Fermi surface, opening new possibilities for novel patterned phases. Non-equilibrium phase transitions to patterned phases, in particular at zero temperature where quantum effects are most relevant, present an interesting paradigm where new universal behavior could be found.

AEA acknowledges Russian Quantum Center for hospitality.

* ribeiro.pedro@gmail.com

[1] M. Cross and P. Hohenberg, Reviews of Modern Physics **65**, 851 (1993).

[2] G. Nicolis and I. Prigogine, *Self-organization in nonequilibrium systems: from dissipative structures to order through fluctuations* (Wiley, 1977) p. 491.

[3] P. Ball, *The Self-Made Tapestry: Pattern Formation in Nature* (Oxford University Press, 1999).

[4] E. Schöll, *Nonequilibrium Phase Transitions in Semiconductors*, Springer Series in Synergetics, Vol. 35 (Springer Berlin Heidelberg, Berlin, Heidelberg, 1987).

[5] R. Kumai, Science **284**, 1645 (1999).

[6] J. Kronjäger, C. Becker, P. Soltan-Panahi, K. Bongs, and K. Sengstock, Physical Review Letters **105**, 090402 (2010).

[7] M. O. Borgh, J. Keeling, and N. G. Berloff, Physical Review B **81**, 235302 (2010).

[8] N. Berloff and J. Keeling, *Physics of Quantum Fluids*, edited by A. Bramati and M. Modugno, Springer Series in Solid-State Sciences, Vol. 177 (Springer Berlin Heidelberg, Berlin, Heidelberg, 2013).

[9] I. Bloch and W. Zwerger, Reviews of Modern Physics **80**, 885 (2008).

[10] N. Strohmaier, D. Greif, R. Jördens, L. Tarruell, H. Moritz, T. Esslinger, R. Sensarma, D. Pekker, E. Altman, and E. Demler, Physical Review Letters **104**, 080401 (2010).

[11] A. Cavalleri, C. Tóth, C. Siders, J. Squier, F. Ráksi, P. Forget, and J. Kieffer, Physical Review Letters **87**, 237401 (2001).

[12] F. Novelli, G. De Filippis, V. Cataudella, M. Esposito, I. Vergara, F. Cilento, E. Sindici, A. Amaricci, C. Giannetti, D. Prabhakaran, S. Wall, A. Perucchi, S. Dal Conte, G. Cerullo, M. Capone, A. Mishchenko, M. Grüninger, N. Nagaosa, F. Parmigiani, and D. Fausti, Nature communications **5**, 5112 (2014).

[13] M. Rigol, V. Dunjko, and M. Olshanii, Nature **452**, 854 (2008).

[14] M. Srednicki, Physical Review E **50**, 888 (1994).

[15] J. Deutsch, Physical Review A **43**, 2046 (1991).

[16] S. Diehl, a. Micheli, a. Kantian, B. Kraus, H. P. Büchler, and P. Zoller, Nature Physics **4**, 878 (2008).

[17] S. Diehl, A. Tomadin, A. Micheli, R. Fazio, and P. Zoller, Physical Review Letters **105**, 015702 (2010).

[18] L. M. Sieberer, S. D. Huber, E. Altman, and S. Diehl, Physical Review Letters **110**, 195301 (2013).

[19] A. Mitra, S. Takei, Y. Kim, and A. Millis, Physical Review Letters **97**, 236808 (2006).

[20] A. Mitra and A. Millis, Physical Review B **77**, 220404 (2008).

[21] S. Takei, W. Witczak-Krempa, and Y. B. Kim, Physical Review B **81**, 125430 (2010).

[22] C.-H. Chung, K. Le Hur, M. Vojta, and P. Wölfle, Physical Review Letters **102**, 216803 (2009).

[23] S. Kirchner and Q. Si, Physical Review Letters **103**, 206401 (2009).

[24] P. Ribeiro, Q. Si, and S. Kirchner, EPL (Europhysics Letters) **102**, 50001 (2013).

[25] P. Werner, T. Oka, and A. Millis, Physical Review B **79**, 035320 (2009).

[26] M. Schiró and M. Fabrizio, Physical Review B **79**, 153302 (2009).

[27] E. Gull, D. R. Reichman, and A. J. Millis, Physical Review B **82**, 075109 (2010).

[28] E. Gull, D. R. Reichman, and A. J. Millis, Physical Review B **84**, 085134 (2011).

[29] G. Cohen, E. Gull, D. R. Reichman, A. J. Millis, and E. Rabani, Physical Review B **87**, 195108 (2013).

[30] H. Aoki, N. Tsuji, M. Eckstein, M. Kollar, T. Oka, and P. Werner, Reviews of Modern Physics **86**, 779 (2014).

[31] M. Schiró and M. Fabrizio, Physical Review Letters **105**, 076401 (2010).

[32] M. Schiró and M. Fabrizio, Physical Review B **83**, 165105 (2011).

[33] M. Eckstein, A. Hackl, S. Kehrein, M. Kollar, M. Moeckel, P. Werner, and F. Wolf, The European Physical Journal Special Topics **180**, 217 (2010).

[34] C. Aron, G. Kotliar, and C. Weber, Physical Review Letters **108**, 086401 (2012).

[35] E. Arrigoni, M. Knap, and W. von der Linden, Physical Review Letters **110**, 086403 (2013).

[36] M. Moeckel and S. Kehrein, Physical Review Letters **100**, 175702 (2008).

[37] M. Eckstein, M. Kollar, and P. Werner, Physical Review Letters **103**, 056403 (2009).

[38] T. Enss and J. Sirker, New Journal of Physics **14**, 023008 (2012).

[39] C. Karrasch, D. M. Kennes, and J. E. Moore, Physical Review B **90**, 155104 (2014).

[40] T. Prosen and M. Žnidarič, Physical Review B **86**, 125118 (2012).

[41] T. Prosen, Physical Review Letters **112**, 030603 (2014).

[42] T. Oka, R. Arita, and H. Aoki, Physical Review Letters **91**, 066406 (2003).

[43] T. Oka and H. Aoki, Physical Review Letters **95**, 137601 (2005).

[44] M. Eckstein, T. Oka, and P. Werner, Physical Review Letters **105**, 146404 (2010).

[45] M. Eckstein and P. Werner, Physical Review Letters **107**, 186406 (2011).

[46] N. Sugimoto, S. Onoda, and N. Nagaosa, Physical Review B **78**, 155104 (2008).

[47] F. Heidrich-Meisner, I. González, K. a. Al-Hassanieh, a. E. Feiguin, M. J. Rozenberg, and E. Dagotto, Physical Review B **82**, 205110 (2010).

[48] Y. Tanaka and K. Yonemitsu, Physical Review B **83**, 085113 (2011).

[49] P. Ribeiro and V. R. Vieira, unpublished.

Supplemental Material: Mott insulator breakdown through pattern formation

Pedro Ribeiro[1], Andrey E. Antipov[2], Alexey N. Rubtsov[1]

[1] *Russian Quantum Center, Novaya street 100 A, Skolkovo, Moscow area, 143025 Russia*
[2] *Department of Physics University of Michigan, Randall Laboratory, 450 Church Street, Ann Arbor, MI 48109-1040*

In this supplemental material we provide some of the details of the analytical analysis performed in the main text of the manuscript. After deriving the Keldysh action we obtain the saddle-point equations used in the mean-field analysis. We provide the explicit expression for the magnetic spin susceptibility.

Keldysh Action

Generating Functional

The generating function in the Keldysh contour γ is defined as

$$Z = \int DC\, e^{i\left[C^\dagger g^{-1} C\right] - i\int_\gamma dz\, \frac{U}{2}\sum_{\boldsymbol{r}}[n_{\boldsymbol{r}}(z)-1]^2} \tag{5}$$

where $C = \begin{pmatrix} c & d_L & d_R \end{pmatrix}^T$ and

$$g^{-1} = \begin{pmatrix} g_\Sigma^{-1} & -V_L & -V_R \\ -V_L^\dagger & g_L^{-1} & 0 \\ -V_R^\dagger & 0 & g_R^{-1} \end{pmatrix} \tag{6}$$

is the inverse of the bare Green's function with

$$\begin{aligned} g^{-1}_{\mathrm{S};\boldsymbol{r},\boldsymbol{r}'}(z,z') &= \delta(z-z')\left(\delta_{\boldsymbol{r},\boldsymbol{r}'} i\partial_z + \tilde{\boldsymbol{t}}_{\boldsymbol{r},\boldsymbol{r}'}\right) \\ g^{-1}_{l;\alpha,\alpha'} &= \delta_{\alpha,\alpha'}\delta(z-z')\left(i\partial_z - \epsilon_{l,\alpha}\right) \\ V_{l;\boldsymbol{r},\alpha} &= v_l \delta_{\boldsymbol{r},\boldsymbol{r}_l} \end{aligned}$$

Using the identity $\frac{U}{2}\sum_{\boldsymbol{r}}(n_{\boldsymbol{r}}-1)^2 = -\frac{3}{4}U\left(\boldsymbol{S}_{\boldsymbol{r}}.\boldsymbol{S}_{\boldsymbol{r}}-1\right)$, with $\boldsymbol{S}_{\boldsymbol{r}} = \frac{1}{2}c^\dagger_{\boldsymbol{r},s}\boldsymbol{\sigma}_{ss'}c_{\boldsymbol{r},s'}$, and inserting a 3-component Hubbard-Stratonovich $\boldsymbol{\phi}$ to decouple the interaction, one obtains, after integrating out the electronic degrees of freedom $Z = \int D\phi\, e^{iS[\phi]}$, where

$$S[\phi] = \frac{1}{2}\left(-\frac{2}{3U}\right)\sum_{\boldsymbol{r}}\int_\gamma dz\, \boldsymbol{\phi}_{\boldsymbol{r}}(z).\boldsymbol{\phi}_{\boldsymbol{r}}(z) - i\,\mathrm{tr}\ln\left[-iG^{-1}\right] \tag{7}$$

with

$$G^{-1} = g_{\mathrm{S}}^{-1} - \Sigma_L - \Sigma_R - \Sigma_\phi \tag{8}$$

$$\Sigma_{l;\boldsymbol{r},\boldsymbol{r}'}(z,z') = |v_l|^2 \sum_\alpha g_{l;\alpha,\alpha}(z,z')\,\delta_{\boldsymbol{r},\boldsymbol{r}_l}\delta_{\boldsymbol{r}',\boldsymbol{r}_l} \tag{9}$$

$$\Sigma_{\phi;\boldsymbol{r},\boldsymbol{r}'} = -\frac{1}{2}\boldsymbol{\sigma}.\boldsymbol{\phi}_{\boldsymbol{r}}(z)\,\delta_{\boldsymbol{r},\boldsymbol{r}'}\delta(z-z') \tag{10}$$

Properties of the reservoirs

As mentioned in the main text the reservoirs are assumed to be metallic leads with a constant density of states within all relevant energy scales. The reservoirs are held in a thermal state characterized by a chemical potential μ_l and a temperature T_l. Under this assumptions we can write

$$\Sigma_l^{R/A}(t,t') \simeq \mp i\Gamma_l\delta(t-t')\,|\boldsymbol{r}_l\rangle\langle\boldsymbol{r}_l| \tag{11}$$

$$\Sigma_l^{K}(t,t') \simeq -2i\Gamma_l F_l(t-t')\,|\boldsymbol{r}_l\rangle\langle\boldsymbol{r}_l| \tag{12}$$

with $\Gamma_l = \pi |v_l|^2 \rho_l(0)$ and

$$F_l(t-t') = \int \frac{d\varepsilon}{2\pi} \tanh\left[\frac{\beta_l}{2}(\varepsilon - \mu_l)\right] e^{-i\varepsilon t} \tag{13}$$

Saddle-Point equations

Variation of the

We define classical and quantum fields as

$$\begin{pmatrix} \boldsymbol{\phi}^i_{c,\boldsymbol{r}}(t') \\ \boldsymbol{\phi}^i_{q,\boldsymbol{r}}(t') \end{pmatrix} = \frac{1}{\sqrt{2}} \begin{pmatrix} 1 & 1 \\ 1 & -1 \end{pmatrix} \cdot \begin{pmatrix} \overrightarrow{\boldsymbol{\phi}^i_{\boldsymbol{r}}}(t') \\ \overleftarrow{\boldsymbol{\phi}^i_{\boldsymbol{r}}}(t') \end{pmatrix} \tag{14}$$

where $\overrightarrow{\boldsymbol{\phi}^i_{\boldsymbol{r}}}(t), \overleftarrow{\boldsymbol{\phi}^i_{\boldsymbol{r}}}(t) = \boldsymbol{\phi}^i_{\boldsymbol{r}}(z)$ (for $z \in \gamma_{\rightarrow}, \gamma_{\leftarrow}$) are respectively the Hubbard-Stratonovich fields in the forwards and backwards parts of the contour. In this way we have that

$$\begin{aligned} -\frac{1}{3U}\sum_{\boldsymbol{r},i}\int_\gamma dz \boldsymbol{\phi}^i_{\boldsymbol{r}}(z)\boldsymbol{\phi}^i_{\boldsymbol{r}}(z) &= -\frac{1}{3U}\sum_{\boldsymbol{r},i}\int dt \begin{pmatrix} \overrightarrow{\boldsymbol{\phi}^i_{\boldsymbol{r}}}(t) \\ \overleftarrow{\boldsymbol{\phi}^i_{\boldsymbol{r}}}(t) \end{pmatrix}^T \begin{pmatrix} 1 & 0 \\ 0 & -1 \end{pmatrix} \begin{pmatrix} \overrightarrow{\boldsymbol{\phi}^i_{\boldsymbol{r}}}(t') \\ \overleftarrow{\boldsymbol{\phi}^i_{\boldsymbol{r}}}(t') \end{pmatrix} \\ &= -\frac{1}{3U}\sum_{\boldsymbol{ri}}\int dt \begin{pmatrix} \boldsymbol{\phi}^i_{c,\boldsymbol{r}}(t) \\ \boldsymbol{\phi}^i_{q,\boldsymbol{r}}(t) \end{pmatrix}^T \begin{pmatrix} 0 & 1 \\ 1 & 0 \end{pmatrix} \begin{pmatrix} \boldsymbol{\phi}^i_{c,\boldsymbol{r}}(t') \\ \boldsymbol{\phi}^i_{q,\boldsymbol{r}}(t') \end{pmatrix} \end{aligned} \tag{15}$$

We proceed to find the saddle-point equations $\delta_{\phi^i_{a,\boldsymbol{r}}(t)} S[\phi] = 0$, resulting in

$$\boldsymbol{\phi}^i_{c,\boldsymbol{r}}(t) = -i\frac{3U}{4}\mathrm{tr}\left\{\frac{1}{\sqrt{2}}\left[G^T\left(t,t+0^+\right) + G^{\bar{T}}\left(t+0^+,t\right)\right]\sigma^i\right\} \tag{16}$$

$$\boldsymbol{\phi}^i_{q,\boldsymbol{r}}(t) = -i\frac{3U}{4}\mathrm{tr}\left\{\frac{1}{\sqrt{2}}\left[G^T\left(t,t+0^+\right) - G^{\bar{T}}\left(t+0^+,t\right)\right]\sigma^i\right\} \tag{17}$$

with G^T and $G^{\bar{T}}$ being the propagators on the forward and backward parts of the contour. Evaluated at the causal solution: $\boldsymbol{\phi}^i_{q,\boldsymbol{r}}(t) = 0$ we obtain

$$\boldsymbol{\phi}^i_{c,\boldsymbol{r}}(t) = -i\frac{3U}{4}\frac{1}{\sqrt{2}}\mathrm{tr}\left[G^K(t,t)\sigma^i\right] \tag{18}$$

From these conditions we obtain, at the saddle-point,

$$\Sigma^{R/A}_{\phi;\boldsymbol{r},\boldsymbol{r}'}(t,t') = -\sqrt{2}\delta(t-t')\delta_{\boldsymbol{r},\boldsymbol{r}'}\frac{1}{2}\boldsymbol{\sigma}.\boldsymbol{\phi}_{c,\boldsymbol{r}}(t) \tag{19}$$

$$\Sigma^K_\phi(t,t') = 0 \tag{20}$$

Equations of motion

From Dyson's equation, i.e. $\left[G^{-1}\right]^{R/A} G^{R/A} = 1$, $\left[G^R\right]^{-1} G^K = \Sigma^K G^A$ and $G^K\left[G^A\right]^{-1} = G^R\Sigma^K$ with ϕ evaluated at the saddle-point conditions, we obtain

$$G^R(t,t') = -i\,\Theta(t-t')\,U(t,t') \tag{21}$$

$$G^A(t,t') = i\,\Theta(t'-t)\,\tilde{U}(t,t') \tag{22}$$

$$G^K(t,t') = U(t,0)\,G^K(0,0)\,\tilde{U}(0,t') + \int_0^t d\tau \int_0^{t'} d\tau'\, U(t,\tau)\,\Sigma^K(\tau,\tau')\,\tilde{U}(\tau',t') \tag{23}$$

where

$$U(t,t') = \mathcal{T} e^{-i\int_{t'}^t d\tau\, K(\tau)} \tag{24}$$

$$\tilde{U}(t,t') = \left[U(t',t)\right]^\dagger = \tilde{\mathcal{T}} e^{i\int_{t'}^t d\tau\, K^\dagger(\tau)} \tag{25}$$

are the time order $\mathcal{T}$ and anti-time ordered $\tilde{\mathcal{T}}$ products and

$$\boldsymbol{K}(t) = \boldsymbol{H}(t) - i\boldsymbol{\Gamma} \tag{26}$$

with

$$\boldsymbol{H}(t) = \sum_{\boldsymbol{r}\boldsymbol{r}'\sigma} |\boldsymbol{r}, s\rangle \left[-\tilde{t}_{\boldsymbol{r},\boldsymbol{r}'} - \frac{1}{\sqrt{2}} \delta_{rr'} \boldsymbol{\sigma}_{ss'} . \boldsymbol{\phi}_{c,\boldsymbol{r}}(t) \right] \langle \boldsymbol{r}', s'| \tag{27}$$

$$\boldsymbol{\Gamma} = \boldsymbol{\Gamma}_L + \boldsymbol{\Gamma}_R \tag{28}$$

$$\boldsymbol{\Gamma}_l = \Gamma_l |\boldsymbol{r}_l\rangle \langle \boldsymbol{r}_l| \tag{29}$$

is a single-particle operator. With this notation, the many-body operator K defined in the main text is given by

$$K = \sum_{\boldsymbol{r}\boldsymbol{r}'ss'} c^\dagger_{\boldsymbol{r}s} \langle \boldsymbol{r}s| \boldsymbol{K} |\boldsymbol{r}'s'\rangle c_{\boldsymbol{r}'s'}.$$

The equation for $G^K(t,t)$, together with the saddle-point conditions constitute a closed set that can be used to describe the evolution of the system at mean-field level:

$$\boldsymbol{\phi}^i_{c,\boldsymbol{r}}(t) = -i\frac{3U}{4}\frac{1}{\sqrt{2}} \mathrm{tr}\left[G^K(t,t)\, \sigma^i \right]$$

$$G^K(t,t) = U(t,0)\, G^K(0,0)\, \tilde{U}(0,t) - 2\pi \int_0^t d\tau \int_0^t d\tau' \sum_l P\left[\frac{1}{(\tau-\tau')} \right] \frac{e^{-i\mu_l(\tau-\tau')} \frac{\pi(\tau-\tau')}{\beta_l}}{\sinh\left[\frac{\pi(\tau-\tau')}{\beta_l} \right]} U(t,\tau)\, \boldsymbol{\Gamma}_l \tilde{U}(\tau', t)$$

where we used $\int \frac{d\varepsilon}{2\pi} \tanh\left[\frac{\beta_l}{2}(\varepsilon - \mu_l) \right] e^{-i\varepsilon t} = e^{-i\mu_l t} \lim_{\eta\to 0} -i \frac{t/\pi}{(\eta^2+t^2)} \frac{\frac{\pi t}{\beta_l}}{\sinh\left(\frac{\pi t}{\beta_l}\right)} = -i\pi e^{-i\mu_l t} P\left(\frac{1}{t}\right) \frac{\left(\frac{\pi t}{\beta_l}\right)}{\sinh\left(\frac{\pi t}{\beta_l}\right)}$.

Steady-state

In a steady-state $\boldsymbol{\phi}_{c,r}(t) = \boldsymbol{\phi}_{c,r}$. Assuming that $\boldsymbol{K}$ is diagonalizable with right and left eigenvectors

$$\boldsymbol{K} |\alpha\rangle = \lambda_\alpha |\alpha\rangle \tag{30}$$

$$\langle\tilde{\alpha}| \boldsymbol{K} = \lambda_\alpha \langle\tilde{\alpha}| \tag{31}$$

such that $\mathrm{Im}\lambda_\alpha < 0$, we can express it as

$$\boldsymbol{K} = \sum_\alpha |\alpha\rangle \lambda_\alpha \langle\tilde{\alpha}| \tag{32}$$

with the identities

$$\sum_\alpha |\alpha\rangle \langle\tilde{\alpha}| = \sum_\alpha |\tilde{\alpha}\rangle \langle\alpha| = 1 \tag{33}$$

$$\langle\alpha\, |\tilde{\alpha}'\rangle = \delta_{\alpha\alpha'} \tag{34}$$

In this basis we also obtain

$$G^R(\omega) = (\omega - \boldsymbol{K})^{-1} = \sum_\alpha |\alpha\rangle (\omega - \lambda_\alpha)^{-1} \langle\tilde{\alpha}| \tag{35}$$

$$G^A(\omega) = \left(\omega - \boldsymbol{K}^\dagger\right)^{-1} = \sum_\alpha |\tilde{\alpha}\rangle \left(\omega - \bar{\lambda}_\alpha\right)^{-1} \langle\alpha| \tag{36}$$

and thus

$$G^K(\omega) = G^R(\omega)\, F(\omega) - F(\omega)\, G^A(\omega) \tag{37}$$

with

$$F(\omega) = \sum_{\alpha\alpha'} |\alpha\rangle \frac{-2i \sum_l \tanh\left[\frac{\beta_l}{2}(\omega - \mu_l) \right] \langle\tilde{\alpha}| \boldsymbol{\Gamma}_l |\tilde{\alpha}'\rangle}{\lambda_\alpha - \bar{\lambda}_{\alpha'}} \langle\alpha'|$$

Quadratic approximation to the action around $\phi = 0$

Second order contribution

The second order approximation of the action around $\phi \simeq 0$ is given by

$$S[\phi] \simeq \frac{1}{2}\left[\phi\pi^{-1}\phi\right] - i\left\{\mathrm{tr}\ln\left[-i\left(G_0^{-1}\right)\right] - \frac{1}{2}\mathrm{tr}\left[\left(G_0\Sigma\right)^2\right]\right\} \tag{38}$$

$$= -i\mathrm{tr}\ln\left[-i\left(G_0^{-1}\right)\right] + \frac{1}{2}\sum_{\boldsymbol{rr'}}\int\frac{d\omega}{2\pi}\begin{pmatrix}\boldsymbol{\phi}^i_{c,\boldsymbol{r}}(t)\\ \boldsymbol{\phi}^i_{q,\boldsymbol{r}}(t)\end{pmatrix}^T\begin{pmatrix}0 & \left[\chi^{-1}\right]^A_{i,j\boldsymbol{rr'}}(t,t')\\ \left[\chi^{-1}\right]^R_{i,j\boldsymbol{rr'}}(t,t') & \left[\chi^{-1}\right]^K_{i,j\boldsymbol{rr'}}(t,t')\end{pmatrix}\begin{pmatrix}\boldsymbol{\phi}^i_{c,\boldsymbol{r}}(t')\\ \boldsymbol{\phi}^i_{q,\boldsymbol{r}}(t')\end{pmatrix} \tag{39}$$

with $G_0^{-1} = G^{-1}\big|_{\phi=0}$. The magnetic susceptibility is defined as $\chi^{ij}_{\boldsymbol{rr'}}(z,z') = -i\left\langle T_\gamma S^i_{\boldsymbol{r}}(z)\, S^j_{\boldsymbol{r'}}(z')\right\rangle$. Explicitly we have

.

$$\left[\chi^{-1}\right]^{ij}_{\boldsymbol{rr'}}(t,t') = \delta_{ij}\begin{pmatrix}0 & -\frac{2}{3U}\delta_{\boldsymbol{rr'}}\delta(t-t') - \Xi^A_{ij;\boldsymbol{rr'}}(t,t')\\ -\frac{2}{3U}\delta_{\boldsymbol{rr'}}\delta(t-t') - \Xi^R_{ij;\boldsymbol{rr'}}(t,t') & -\Xi^K_{ij;\boldsymbol{rr'}}(t,t')\end{pmatrix}$$

where Ξ denotes the bubble-like diagrams

$$\Xi^R_{\boldsymbol{rr'}}(t,t') = -i\frac{1}{2}\mathrm{tr}\left[G^A_{0;\boldsymbol{r'r}}(t',t)\,G^K_{0;\boldsymbol{rr'}}(t,t') + G^K_{0;\boldsymbol{r'r}}(t',t)\,G^R_{0;\boldsymbol{rr'}}(t,t')\right]$$

$$\Xi^A_{rr'}(t,t') = -i\frac{1}{2}\mathrm{tr}\left[G^R_{0;\boldsymbol{r'r}}(t',t)\,G^K_{0;\boldsymbol{rr'}}(t,t') + G^K_{0;\boldsymbol{r'r}}(r't',rt)\,G^A_{0;\boldsymbol{rr'}}(t,t')\right]$$

$$\Xi^K_{rr'}(t,t') = -i\frac{1}{2}\mathrm{tr}\left[G^A_{0;\boldsymbol{r'r}}(t',t)\,G^R_{0;\boldsymbol{rr'}}(t,t') + G^R_{0;\boldsymbol{r'r}}(t',t)\,G^A_{0;\boldsymbol{rr'}}(t,t') + G^K_{0;\boldsymbol{r'r}}(t',t)\,G^K_{0;\boldsymbol{rr'}}(t,t')\right]$$

Assuming a steady state condition we obtain, for the retarded component

$$\Xi^R_{rr'}(\omega) = \Xi^{(1)}_{rr'}(\omega) + \bar{\Xi}^{(2)}_{rr'}(-\omega) + \Xi^{(2)}_{rr'}(\omega) + \bar{\Xi}^{(1)}_{rr'}(-\omega)$$

$$\Xi^{(1)}_{rr'}(\omega) = -\sum_{\alpha\beta}\sum_l\left\langle r'\left|\tilde{\beta}\right\rangle\langle\beta\,|r\rangle\langle r\,|\alpha\rangle\,A^l_{\alpha r'}\,I_l\left(\bar{\lambda}_\beta+\omega,\lambda_\alpha\right)\right.$$

$$\Xi^{(2)}_{rr'}(\omega) = -\sum_{\alpha\beta}\sum_l\langle r'\,|\alpha\rangle\langle r\,|\beta\rangle\left\langle\tilde{\beta}\,|r'\right\rangle A^l_{\alpha r}\,I_l\left(\lambda_\beta-\omega,\lambda_\alpha\right)$$

with

$$I_l(z,z') = \frac{1}{\pi}\frac{\psi^{(0)}\left[\frac{1}{2} - i\mathrm{sgn}\left(\mathrm{Im}z'\right)\frac{\beta_l(z'-\mu_l)}{2\pi}\right] - \psi^{(0)}\left[\frac{1}{2} - i\mathrm{sgn}\left(\mathrm{Im}z\right)\frac{\beta_l(z-\mu_l)}{2\pi}\right]}{z-y}$$

$$A^l_{\alpha r} = \sum_{\alpha'}\frac{\langle\tilde{\alpha}|\,\boldsymbol{\Gamma}_l\,|\tilde{\alpha}'\rangle\,\langle\alpha'\,|r\rangle}{\lambda_\alpha - \bar{\lambda}_{\alpha'}}$$

with $\psi^{(0)}(z) = \partial_z \ln\Gamma(z)$ being the logarithmic derivative of the Gamma function.